Torque-Bias Profile for Improved Tracking of the Deep Space Network Antennas

W. Gawronski[1], J. J. Beech-Brandt[2], H. G. Ahlstrom, Jr.[3], and E. Maneri[4]

[1]Communications Ground Systems Section, Jet Propulsion Laboratory
California Institute of Technology
4800 Oak Grove Drive, Pasadena, CA 91109 USA
Tel: +1 (818) 354-1783; E-mail: wodek.k.gawronski@jpl.nasa.gov

[2]Department of Mathematics and Statistics, The King's Buildings, University of Edinburgh
Edinburgh, Scotland, UK EH9 3JZ
Tel: +44 (131) 650 5067; E-mail: jason@maths.ed.ac.uk

[3]Jet Propulsion Laboratory, California Institute of Technology, MS 238-528
4800 Oak Grove Drive, Pasadena, CA 91109 USA
Tel: +1 (818) 354-1847; Fax: +1 (818) 393-0207; E-mail: harlow.g.ahlstrom-jr@jpl.nasa.gov

[4]Jet Propulsion Laboratory, California Institute of Technology, MS 238-528
4800 Oak Grove Drive, Pasadena, CA 91109 USA
Tel: +1 (818) 354-2809; Fax: +1 (818) 393-0207; E-mail: erin.j.maneri@jpl.nasa.gov

Abstract

Measurements at the drives of the NASA Deep Space Network (DSN) antennas indicated that the small gap between gear teeth was causing backlash at the gearboxes and elevation bullgear. Left uncorrected, backlash will deteriorate the antenna's pointing precision. Backlash is observed not only in antennas and telescopes [1, 2], but also in precision instruments [3-6] and robots [7, 8]. Often, to reduce backlash impact on the closed-loop precision, anti-backlash controllers are designed [9-11]. At DSN, the backlash was eliminated by implementing two identical drives that impose two non-identical torques (a.k.a. torque bias, or counter-torque). The difference between these two torques depends on the antenna load, and is shaped by the drive's electronic circuits. The paper explains the shaping principles of the circuit, and shows how the circuits can be modified to improve the antenna dynamics under external disturbances.

Keywords: Antenna mechanical factors; motor drives; friction; gears; torque control

1. Introduction

Gearboxes and gears are two critical components of the NASA Deep Space Network (DSN) antenna drives. A backlash phenomenon is observed when one gear rotates through a small angle without causing a corresponding movement in the gear it is driving. This "beating" in the drives eventually causes gear wear and deterioration of the antenna's tracking precision. In order to maintain pointing precision, the backlash is eliminated by implementing an additional drive with a specified torque difference between it and the original. The torque difference is called a torque bias, or counter-torque. With a two-motor configuration (see Figure 1), backlash clearance will occur at one drive while the other is still coupled, and the antenna dynamics will be controlled by the latter drive. The effectiveness of the two-motor approach depends on the amount of torque bias applied at the drives, which depends on the antenna load. It should be large enough to lead the antenna through the gap for the maximum allowable torque load, but small enough that it will not cause excessive local stress, friction, and wear.

High and steady loads do not need a torque bias, since the backlash is observed for low and reversing-axis loads, only. Time-varying loads, such as wind gusts, can produce high torques that become very low within a short period of time, which cause a backlash gap when the torque-bias dynamics are too slow. Reversing loads from wind gusting were observed and recorded at the DSS13 antenna site. Dynamics of the torque-bias-shaping loop that will remedy the antenna-tracking-precision situation are derived in this paper.

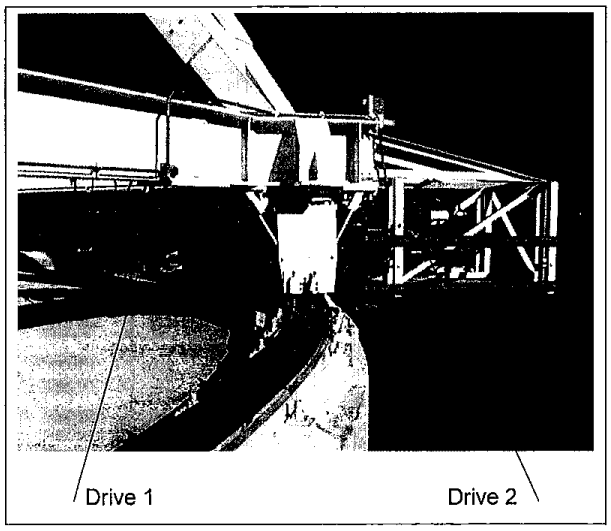

Figure 1a. The azimuth drive of the 34-meter antenna: the two-drive configuration.

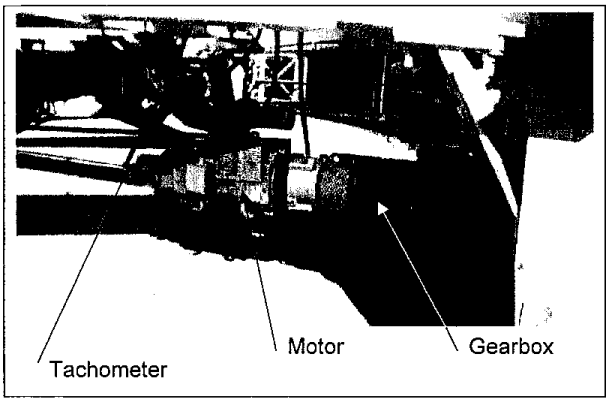

Figure 1b. A close look at a single drive in the azimuth drive of the 34-meter antenna.

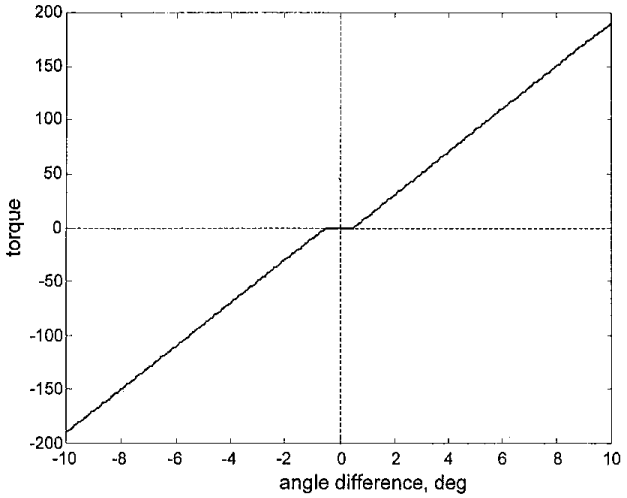

Figure 2. The backlash function, showing the relationship between the gear-angle difference and the torque.

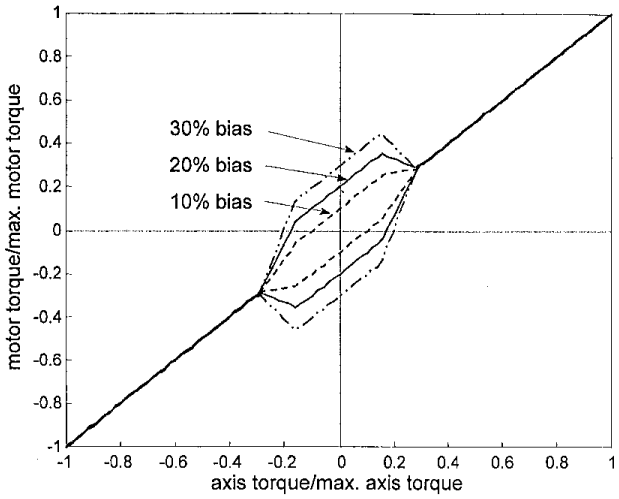

Figure 3. The motor torque as a function of the axial torque, for 10% (dashed line), 20% (solid line), and 30% (dot-dashed line) torque bias. The upper lines represent drive 1; the lower lines represent drive 2.

2. Backlash and Its Prevention

Consider a simple gearbox, with two gears rotating in opposite directions. Let the angle of rotation of the first gear be β_1, let that of the second gear be β_2, let the gearbox ratio be N, and let the gearbox stiffness (measured at the second gear) be k. In this case, the relationship between the gearbox rotation and the torque, T, at the second gear is as follows:

$$T = \begin{cases} 0 & \text{for } |\Delta\beta| \le b \\ k(\Delta\beta - b) & \text{for } \Delta\beta > b \\ k(\Delta\beta + b) & \text{for } \Delta\beta < -b \end{cases}, \qquad (1)$$

where $\Delta\beta = \beta_2 - \beta_1/N$, and b is the size of the backlash gap, measured at the second gear. A plot of torque versus angle difference $\Delta\beta$ is shown in Figure 2, for $b = 1$ and $k = 20$. It is clear from Equation (1) that if the angle difference of two gears is smaller than the backlash gap, b, the gear motion is discontinuous, and the gear teeth impact with each other.

Implementing two driving gears, of torques T_1 and T_2 (which differ by the amount of ΔT), instead of a single one will minimize the impact at the discontinuity. This difference, called torque bias or counter-torque, will continually drive the antenna, even if one gear is in backlash. This principle of *torque sharing* is used in beam-waveguide (BWG) antenna design.

The question remains as to how large the torque bias must be to prevent backlash. If the stiffness of the gearbox is k and the backlash gap is b, the torque bias, ΔT, should be greater than $2kb$. But ΔT is a function of the load applied to the gears as well: a bias is not required if the torque load is high ($T_1 \cong T_2 \gg \Delta T$), because the angle difference is large and backlash is not observed (even when $\Delta T = 0$). Plots of the existing profile of motor torque versus axial load (as a percentage of the maximum load) are shown in Figure 3 for 10, 20, and 30 percent of the bias. The bias is shaped

such that it is the largest for the low loads, and phases out for higher loads.

In the event of dynamic loading, such as wind gusts, the optimum magnitude of the torque bias is not obvious. During dynamic loading, the torque difference determined for the steady-state case may not be large enough to prevent the backlash, and assuming a higher counter-torque may lead to premature wear. Additionally, quickly varying loads, with small, steady components, may cause backlash in both gears simultaneously, despite the non-zero torque bias. Thus, the torque-bias time response is also an important design factor.

Torque-shaping analysis helps to determine the value of the bias, the rate of phase-out, and the dynamics of the counter-torque circuit.

3. Friction

Friction is a torque that always opposes motion. The friction torque, T_f, depends on the relative velocity, v, of the moving surfaces. After motion begins, the friction torque is constant, and is referred to as the Coulomb friction torque, T_c. At a relative speed of zero, the friction torque, T_f, is equal and opposite to the applied torque, T_o, unless the applied torque is larger than the stiction torque, $T_s > 0$. The latter is the torque at the moment of breakaway, and is larger than the Coulomb torque. A diagram of the friction torque versus the relative velocity is shown in Figure 4. The velocity threshold, $v_t > 0$, is small, and the friction torque is

$$T_f = \begin{cases} -T_c \operatorname{sign}(v) & \text{for } |v| > v_t \\ -\min(|T_o|, T_s)\operatorname{sign}(T_o) & \text{for } |v| \le v_t \end{cases}, \qquad (2)$$

where $y = \operatorname{sign}(x)$ denotes a sign function: $y = 1$ for $x > 0$, $y = -1$ for $x < 0$, and $y = 0$ for $x = 0$. This equation states that if the surfaces in contact develop measurable relative velocity, such that $v > v_t$, the friction torque is constant, and directed opposite to the relative speed. If the relative velocity is small (within the threshold $v \le v_t$) the friction torque does not exceed the stiction torque or the applied torque, and is directed opposite to the applied torque. The velocity threshold, v_t, is included for numerical purposes, since the probability of determining the time of exact zero-crossing is zero ($v(i)$ is assumed zero within the threshold).

In order to determine the friction torque, T, the Coulomb friction torque, T_c, the stiction (breakaway) torque, T_s, the applied torque, T_o, and the wheel rate, v, must be known.

The *Coulomb friction torque* is proportional to the normal force at the surface F:

$$T_c = \mu r F, \qquad (3)$$

where r is the wheel radius and μ is the friction coefficient. For hard steel, $0.0012 < \mu < 0.002$.

The *stiction (breakaway) torque* is most often assumed to be slightly higher than the Coulomb friction:

$$T_s = \alpha T_c, \qquad \alpha = 1.2 - 1.3. \qquad (4)$$

The *total applied torque* is determined as follows. Let the discrete state-space equation of the open-loop antenna be

$$x(i+1) = Ax(i) + B_u u(i) + B_f T(i), \qquad (5a)$$

$$v(i) = Cx(i), \qquad (5b)$$

where v is the antenna's angular rate and T is the friction torque (either of azimuth or elevation axis), and $(A, [B_u, B_f], C)$ is the state-space representation of the open-loop antenna. When the antenna velocity is within the threshold $|v| \le v_t$, v is assumed to be zero. Multiplying the left-hand side of Equation (5a) by C yields

$$v(i+1) = Cx(i+1) = CAx(i) + CB_u u(i) + CB_f T(i). \qquad (6)$$

But $v(i+1) = 0$, and thus

$$T(i) = -\frac{C}{CB_f}\left[Ax(i) + B_u u(i)\right], \qquad (7)$$

and the applied torque, T_o, is equal in magnitude but opposite to the torque, T, i.e.,

$$T_o(i) = \frac{C}{CB_f}\left[Ax(i) + B_u u(i)\right]. \qquad (8)$$

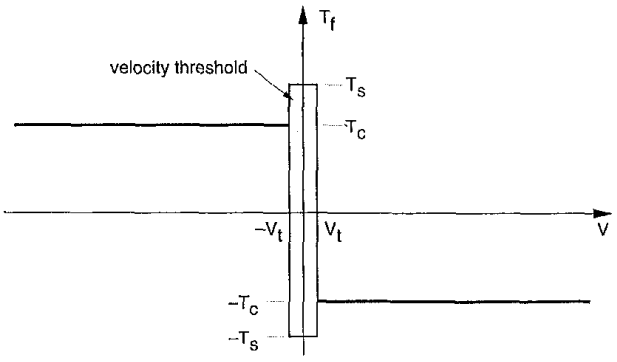

Figure 4. The friction torque as a function of the relative velocity of the moving surfaces.

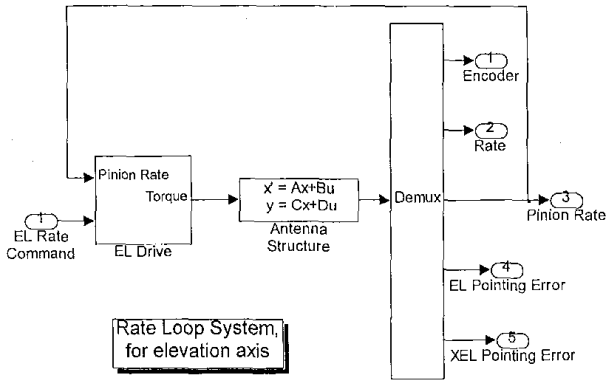

Figure 5. A *Simulink*® model of the elevation rate-loop system.

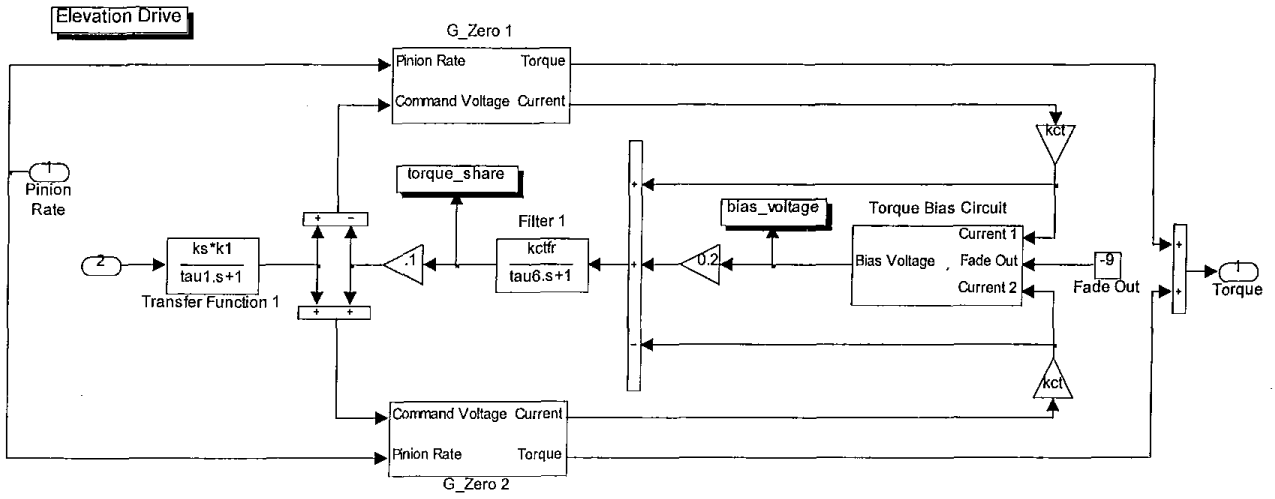

Figure 6. A *Simulink*® model of the elevation drive.

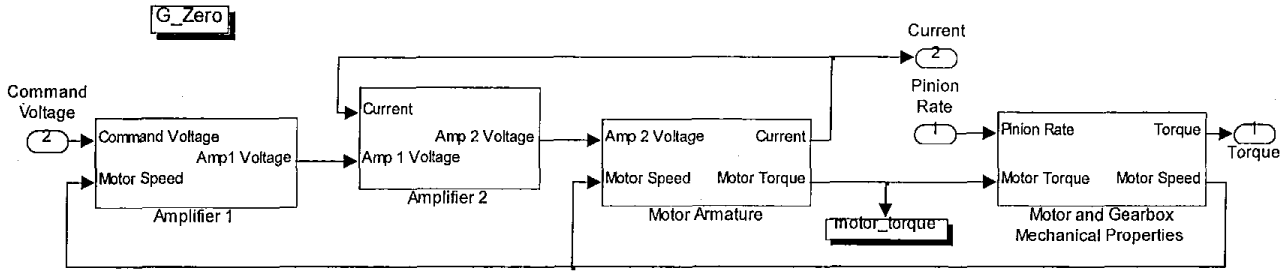

Figure 7. A *Simulink*® model of the motor, gearbox, and amplifier (system G_o).

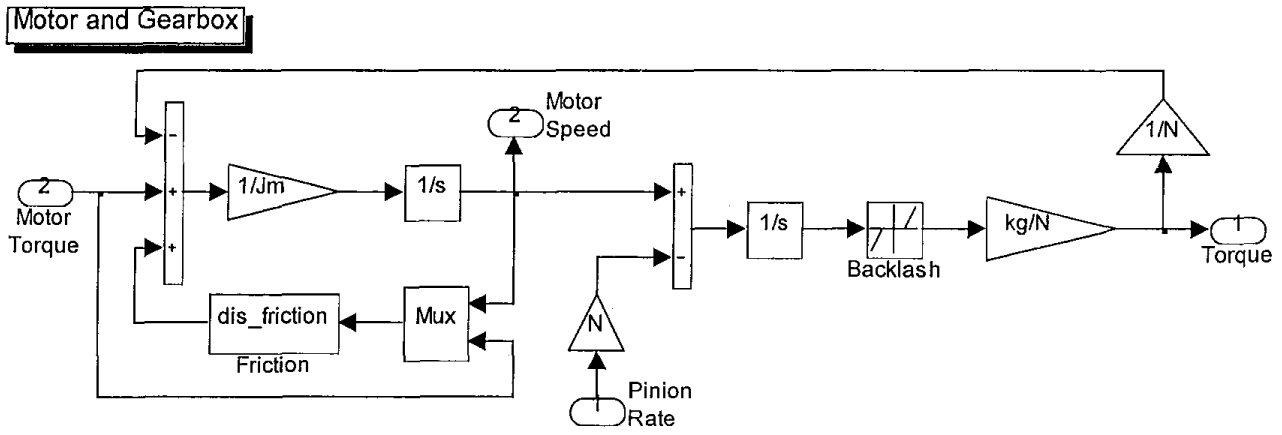

Figure 8. A *Simulink*® model of the mechanical properties of the motor and gearbox.

4. The Rate-Loop Model, with Friction and Backlash

The motions of the antenna's elevation and azimuth axes are uncoupled, and can therefore be analyzed independently. The *Simulink*® model of the elevation rate-loop system is shown in Figure 5 (the following block diagrams are also *Simulink*® diagrams). The model contains the antenna structure with an elevation-rate input. The outputs are the elevation encoder, elevation rate, elevation pinion rate, and elevation and cross-elevation pointing-error measurements. The antenna structure model was obtained from the DSS13 finite-element model, as described in [12, 13]. The elevation-drive model, which consists of the elevation-rate input, elevation pinion-rate inputs, and elevation torque output, is shown in Figure 6.

The drive consists of two motors (with gearboxes), denoted G_o, and the torque-share circuit. The notation here is consistent with that of references [12, 13]. The block diagram of the subsys-

tem G_o is shown in Figure 7. It consists of two amplifiers, a motor armature, and a gearbox. The amplifiers and the motor armature are the same as those described in [12, 13]. However, the gearbox model differs from the linear one in that it includes nonlinear friction and backlash models (see Figure 8). The friction torque in this model depends on the motor torque and motor speed, as described in Equation (2). In the backlash model, the torque depends on the difference between the motor and the pinion angle, as in Equation (1). The torque-share circuit, shown in Figure 6, will be described below.

The accuracy of the rate-loop model was verified experimentally. Open-loop tests were conducted at the DSS26 antenna to compare the measured antenna dynamics with the simulated dynamics of the model that includes backlash and friction. The test data were used to determine the amount of friction and the backlash angle. The rate-loop experiments were conducted with a square-wave input of period 6.3 s and amplitude 0.013°/s. Two tests were conducted: one with zero torque bias, and another with a torque bias of 15% of the maximum motor torque (the maximum torque is 308 kgm (26700 lb in): thus, torque bias was set at 46 kgm (4000 lb in)).

For brevity of presentation, we consider the elevation axis only.

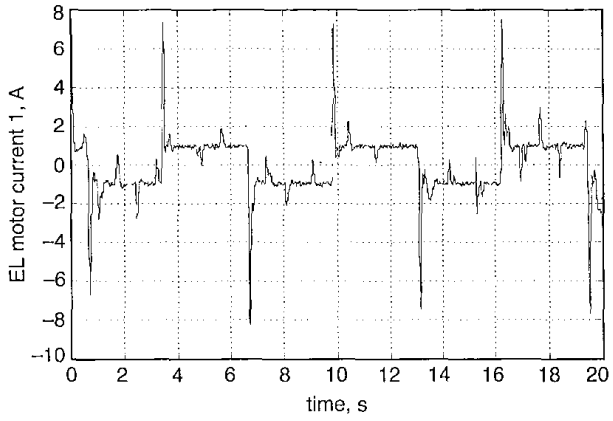

Figure 9a. The measured motor currents for zero torque bias.

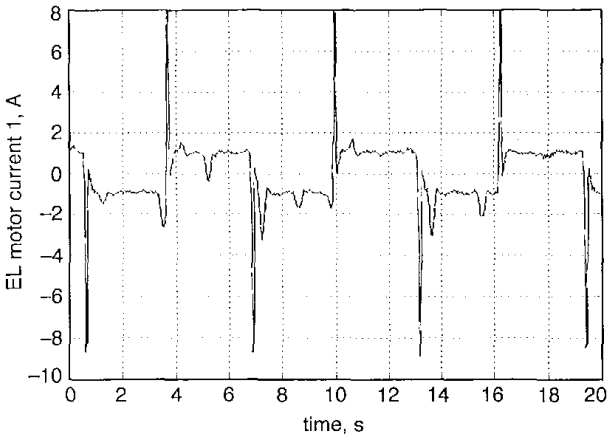

Figure 9b. The simulated motor currents for measured torque bias.

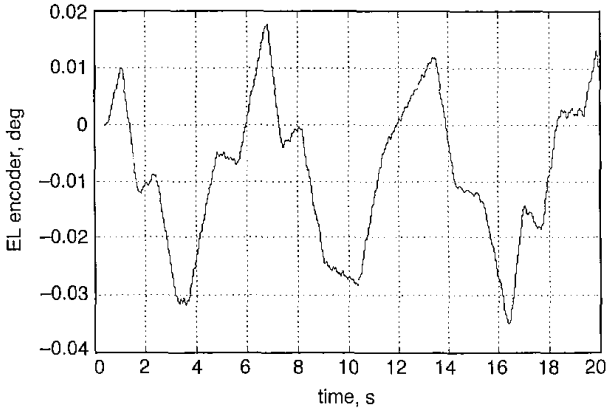

Figure 10a. The measured encoder readings for zero torque bias.

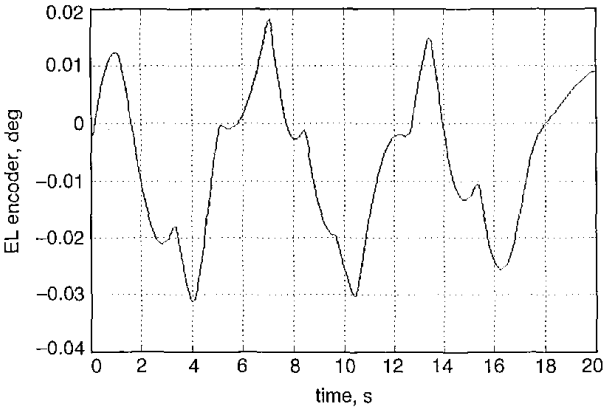

Figure 10b. The simulated encoder readings for zero torque bias.

With zero torque bias, the measured motor current (excited by the square wave) and measured encoder reading are shown in Figures 9a and 10a, respectively. The simulated motor current and simulated encoder readings are shown in Figures 9b and 10b. These plots show satisfactory coincidence between the field data and the simulation results. In addition, the measured motor currents, which are proportional to the motor torques, were used to determine the frictional torques.

The constant current in Figure 9a measures ±1 A, and corresponds to the constant antenna rate, since inertial forces are not present and the motor's effort is totally dedicated to overcoming the frictional forces. The 1 A current corresponds to a 61 kgm (5300 lb in) motor torque, or a 9.1×10^{5} kgm (7.9×0^{7} lb in) axis torque, which is the measure of the frictional torque.

For 15% torque bias, the plots of measured and simulated motor currents and encoder readings are given in Figures 11a,b and 12a,b, respectively. This situation differs from that of the zero-torque-bias case, in that the encoder shows less chaotic movement of the antenna (c.f., Figures 10 and 12), and the motor-torque plots indicate the presence of the torque bias (their mean values are non-zero and have opposite sign (c.f., Figures 9 and 11)).

5. Modifications of the Bias Profile

The torque-share circuit is shown in Figure 13. Given an antenna load value, the circuit will determine an appropriate torque bias. Therefore, the load (motor current, i) is the circuit input; the fade-out voltage, f_o, is an additional voltage input that shapes the torque bias; and the circuit output is the torque bias, v_b, given in volts. The relationship between the current, i (the sum of the currents at motors one and two), and the bias voltage, v_b, follows from the block diagram in Figure 13:

$$v_b = k_p \,\mathrm{sat}\left(G_2 f_o + G_4 \left|G_3 i\right|\right), \tag{9}$$

where G_2, G_3, and G_4 are the transfer functions 2, 3, 4, respectively, and k_p is the bias pot ($k_p = 0.8$). The parameters of the transfer functions are given in Table 1. The saturation function, sat, is defined as follows:

$$\mathrm{sat}(v) = \begin{cases} v_u & \text{if } v > v_u \\ v_l & \text{if } v < v_l \\ v & \text{elsewhere} \end{cases}, \tag{10}$$

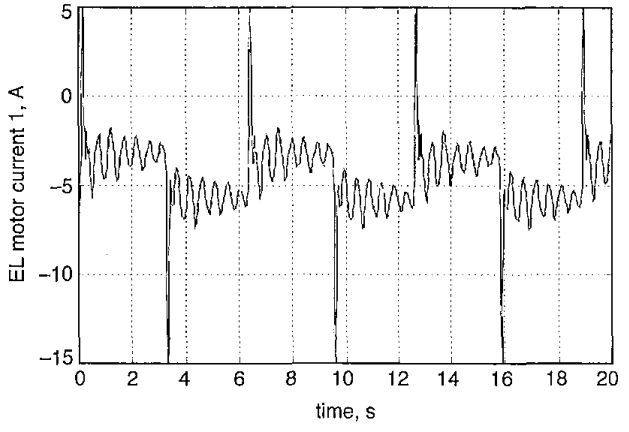

Figure 11a. The measured motor currents for 15% torque bias.

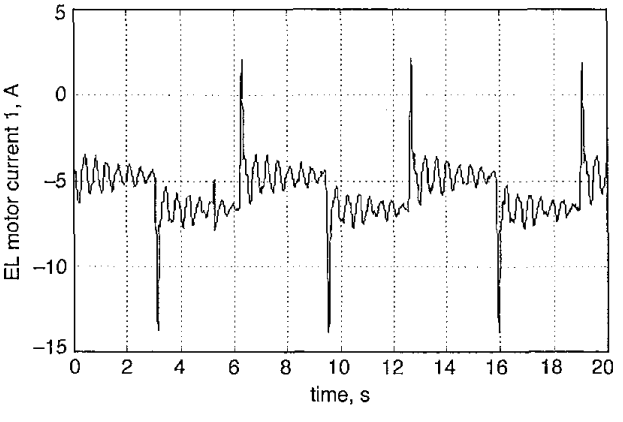

Figure 11b. The simulated motor currents for 15% torque bias.

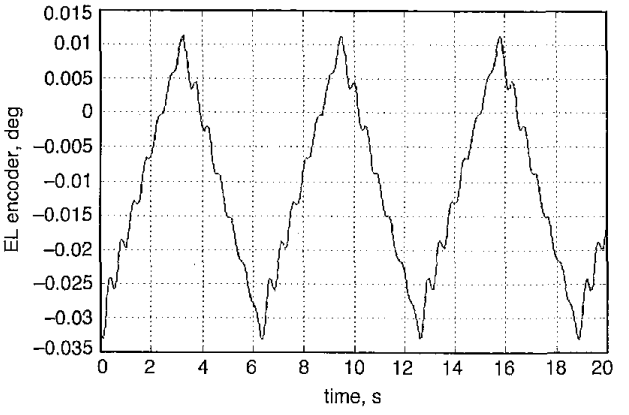

Figure 12a. The measured encoder readings for 15% torque bias.

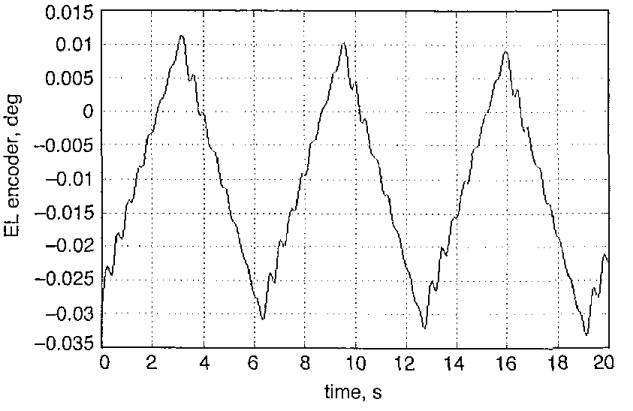

Figure 12b. The simulated encoder readings for 15% torque bias.

where the upper and lower limits of saturation are $v_u = 13$ V and $v_l = 0$ V.

Note that the transfer functions, G_2 and G_4 of Figure 13, are proportional, that is,

$$G_4 = k_2 G_2, \tag{11}$$

where $k_2 = 2.6$. Substituting Equation (11) into Equation (9) yields

$$v_b = k_p \,\mathrm{sat}\left[G_2\left(f_o + k_2 \left|G_3 i\right|\right)\right]. \tag{12}$$

The steady-state torque profile is obtained by replacing G_2 and G_3 with their corresponding dc gains:

$$G_3(0) = -1 \tag{13a}$$

and

$$g_2 = G_2(0) = -3.20. \tag{13b}$$

Thus, the steady-state bias voltage of Equation (12) becomes

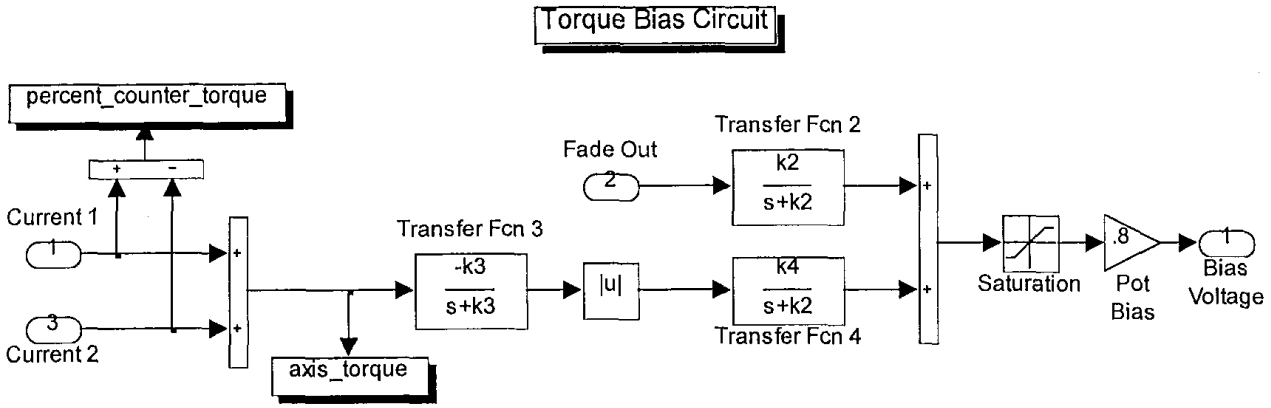

Figure 13. A *Simulink*® model of the torque-share circuit.

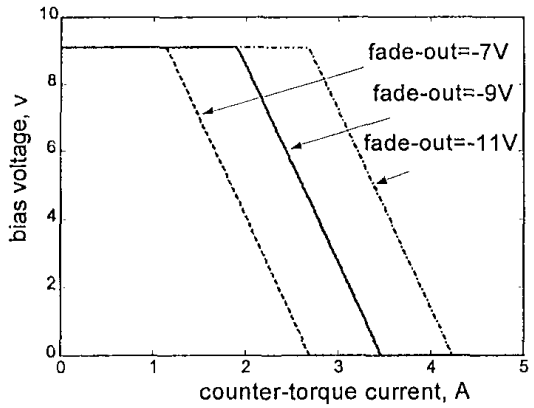

Figure 14a. The bias voltage as a function of the axis torque for the three different fade-out voltages: −7 V (dashed line), −9 V (solid line), and −11 V (dashed-dot line).

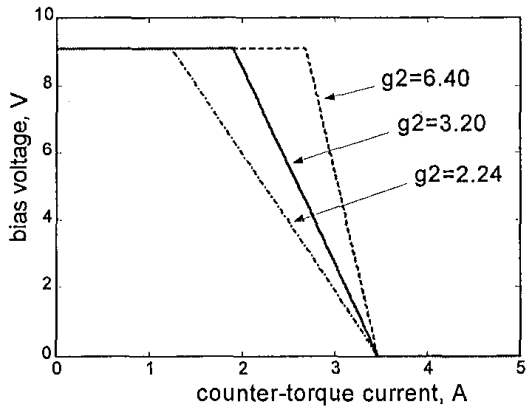

Figure 14c. The bias voltage as a function of the axis torque for three cases of dc gain: nominal gain, $g_2 = -3.20$ (solid line); two-fold increased gain, $g_2 = -6.40$ (dashed line); and the reduced gain, $g_2 = -2.24$ (dashed-dotted line).

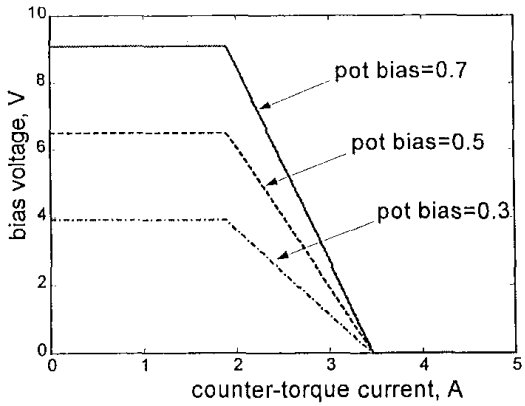

Figure 14b. The bias voltage as a function of the axis torque for the bias pot values of 0.3 (dashed-dot line), 0.5 (dashed line), and 0.7 (solid line).

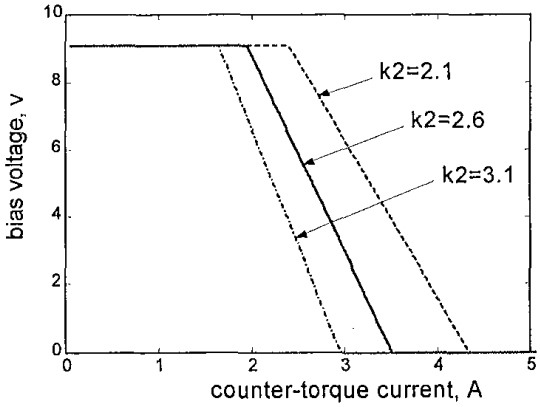

Figure 14d. The bias voltage as a function of the axis torque for the gain $k_2 = 2.1$ (dashed line), $k_2 = 2.6$ (solid line), and $k_2 = 3.1$ (dash-dotted line).

$$v_b = k_p \,\mathrm{sat}\left[g_2\left(f_o + k_2|i|\right)\right]. \qquad (14)$$

The plot of v_b versus i (which is proportional to the axis torque) for $k_p = 0.7$, $g_2 = -3.20$, $f_o = -9\,\mathrm{V}$, and $k_2 = 2.6$ (as implemented at DSS13) is shown in Figure 14a as a solid line.

The bias can be shaped in three ways:

- extending the constant value of the bias;
- changing the constant value of the bias;
- changing the slope of the bias.

From Equation (14), it follows that the first modification (extending the constant value of the bias) is obtained by changing the value of the fade-out voltage, f_o. The bias profiles for three different fade-out voltages are shown in Figure 14a: the dashed line represents a fade-out voltage of $-7\,\mathrm{V}$, the solid line represents $-9\,\mathrm{V}$, and the dashed-dot line represents a fade-out voltage of $-11\,\mathrm{V}$. A greater absolute value of the voltage corresponds to a wider constant value of bias.

Table 1. Transfer-function parameters.

Block	Variable	Old Model	New Model
Filter 1	kctfr	4.54	66.67
	tau6	1.369	8.889
Transfer function 1	ks	0.8	
	k1	716.197	
	tau1	6.37×10^{-3}	
Transfer function 2	k2	-3.502	-2.114
	s2	1.093	0.8895
Transfer function 3	k3	2	3.831
Transfer function 4	k4	$2.6k_2$	$1.617k2$

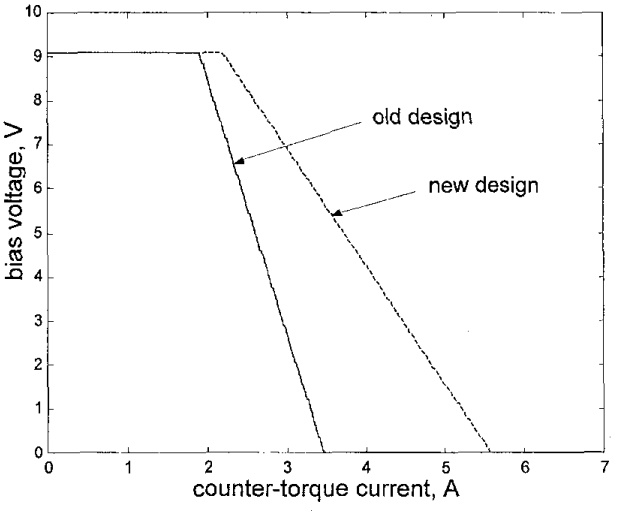

Figure 15. The bias voltage as a function of the axis torque for $g_2 = -2.38$ and $k_2 = 1.617$ (dashed line), and for the existing gains (solid line).

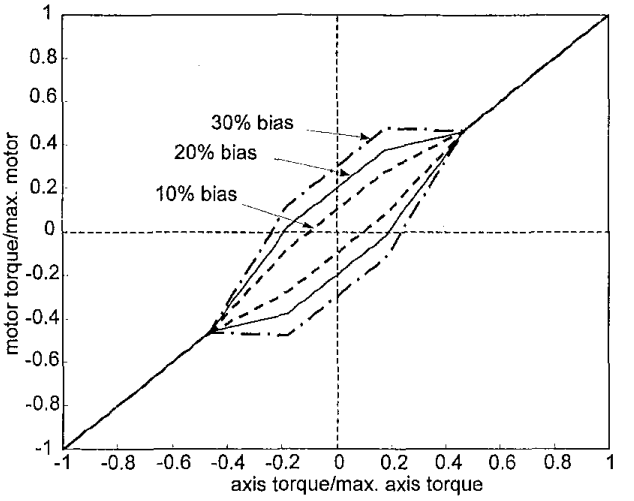

Figure 16. The modified profile of the motor torque as a function of the axial torque, for 10% (dashed line), 20% (dot-dashed line), and 30% (solid line) torque bias.

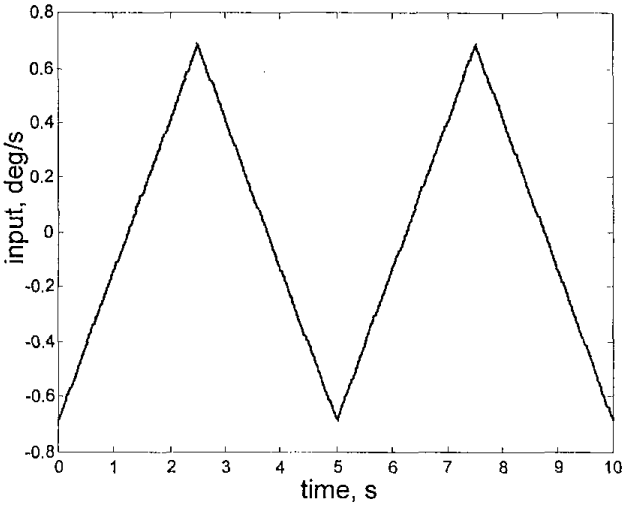

Figure 17. The test signal.

Inspection of Equation (14) suggests the second modification, varying the constant value of torque bias by varying the bias potentiometer value, k_p. The plots of bias voltage vs. counter-torque current for bias pot values of 0.3 (dashed-dot line), 0.5 (dashed line), and 0.7 (solid line) are shown in Figure 14b. The plot shows that larger bias-potentiometer settings result in larger bias voltages.

The slope is modified by varying the gain, g_2, of the transfer function TF2. This is illustrated in Figure 14c with three cases of gain scaling: the nominal gain, $g_2 = -3.20$ (solid line); the two-fold increase in gain, $g_2 = -6.40$ (dashed line); and the reduced gain, $g_2 = -2.24$ (dashed-dotted line). The plots show that smaller gains yield smaller slopes.

Finally, Equation (14) clarifies the relationship between bias voltage and gain, k_2, which is illustrated in Figure 14d where the slope and horizontal extension of the bias are varied simultaneously after modifying k_2.

To prevent backlash under extreme dynamic loads, a flatter bias voltage is ideal. Gains g_2 and k_2 were modified according to the relationships above. The dashed line in Figure 15 shows the bias-voltage profile for $g_2 = -2.38$ and $k_2 = 1.617$. This slope is smaller when compared with the nominal, solid line. The resulting profile (as a percentage of the maximum torque) is shown in Figure 16 for 10, 20, and 30 percent of the bias. Compare this profile with that of the existing torque bias (Figure 4), and note the sharp decline for the existing configuration, compared to the mild slopes of the modified design.

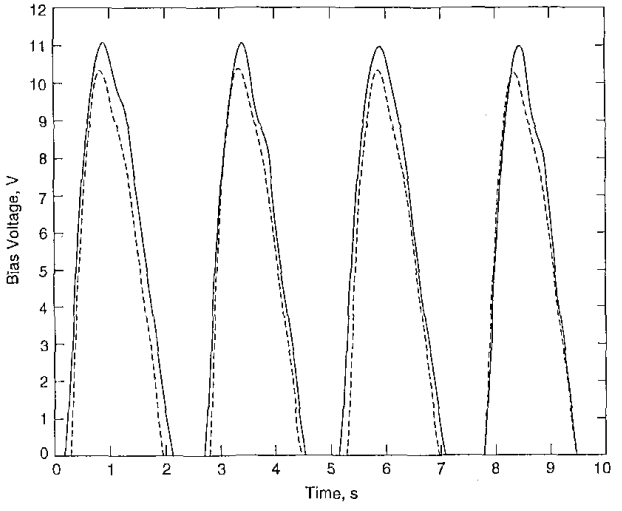

Figure 18. The bias voltage under the test signal for the old circuit design: from field tests (solid line) and from analysis (dashed line).

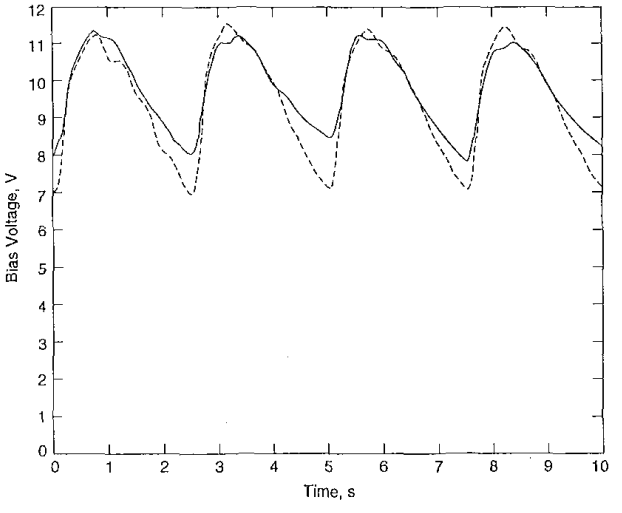

Figure 19. The bias voltage under the test signal for the new circuit design: from field tests (solid line) and from analysis (dashed line).

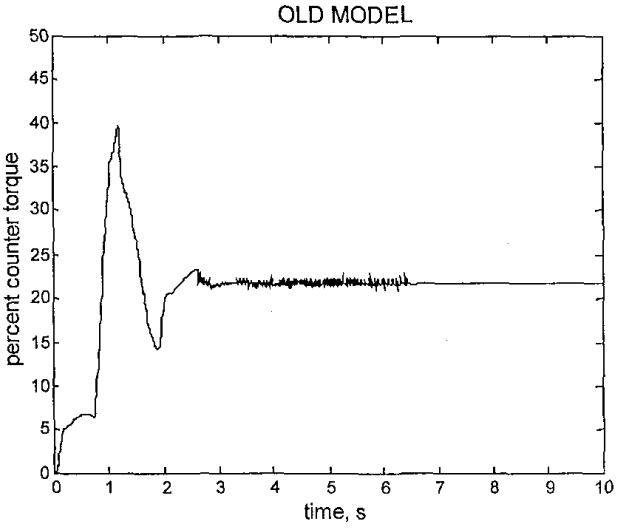

Figure 20a. The counter-torque dynamics for $\tau_6 = 0.73$ s, $k_{ctfr} = 3.31$.

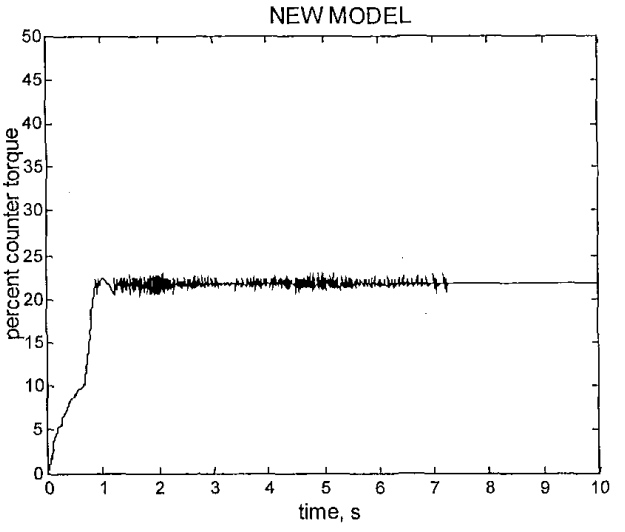

Figure 20b. The counter-torque dynamics for $\tau_6 = 0.1125$ s, $k_{ctfr} = 48.67$.

The performance of the old and new rate-loop models have been verified analytically and in the field. The bias voltage was used as an indicator of the quality of the design. For best results, the bias should remain at the maximum value; in an acceptable design, the bias would always be non-zero; a poor design is characterized by a bias that remains even at small angles, causing backlash. The differences between these designs can be exposed during high loads that vary abruptly. Therefore, a sawtooth wave, of amplitude 0.685°/s (85% of the maximum rate) and period 5 s, was chosen as a test signal to be applied at the antenna-rate loop input (see Figure 17). The bias-voltage response of the old design to a sawtooth input is shown in Figure 18, with the solid line (measured at the DSS26 antenna) and dashed line (the results of simulation using an analytical model). Both plots show a bias voltage that varies extensively, and remains at zero for significant periods. The maximum biases were 11.2 V (field data) and 10.4 V

(analysis), which are 86% and 80% of the maximum bias, respectively. The test results for the new design are shown in Figure 19 by the solid line (field data) and the dashed line (simulations). Both show a non-zero bias that varies from 8.0 to 11.4 V (field data), and from 7.2 to 11.6 V (analysis). This translates to 62-87% of maximum bias (field data), and into 56-88% of maximum bias (analysis). These data show that the bias torque performance was significantly improved.

6. Improvements of the Bias-Torque Dynamics

Filter 1 in the drive block diagram (Figure 6) is responsible for the torque-bias dynamics. Its transfer function is given by

$$G_1 = \frac{k_{ctfr}}{1+\tau_6 s}, \qquad (15)$$

with gain $k_{ctfr} = 3.31$ and time constant $\tau_6 = 0.73$ s. These filter constants were carried over from the existing design.

Let i_1 and i_2 denote the currents of motors 1 and 2, respectively. The torque bias is proportional to their difference: $\Delta i = i_2 - i_1$. An experiment was conducted in which a rate command of zero was applied, and the relative torque bias, $(\Delta i / i_{\max}) \times 100\%$, was recorded. The initial torque bias was set to zero, and in the first period of antenna response, the torque bias increased to its nominal value (22%). The response is illustrated in Figure 20a, with a (nominal) time constant of $\tau_6 = 0.73$ s and a variable gain k_{ctfr} of 3.31. The figure shows that overshoot is significant, and the settling time is greater than 2 s.

After examining the impact of Filter 1's time constant and gain on the counter-torque dynamics, $\tau_6 = 0.1125$ s and $k_{ctfr} = 48.67$ were chosen as the new values. Counter-torque dynamics resulting from the above parameters are shown in Figure 20b, where overshoot (0%) and settling time (0.8 s) have improved significantly.

7. Conclusions

This project involved measurement, modeling, and simulation of the backlash and friction in the 34 m DSN antenna. The existing torque-shaping circuit was analyzed, and a new bias-torque profile was developed. The new profile, shaped with Filter 1 of the drive system, had flatter slopes, which softened the torque-bias variations regardless of load. The torque-bias overshoot improved from 80% to 0%, and the settling time shortened from 2.4 s to just 0.8 s. Field tests confirmed the improved antenna performance with the new torque-shaping circuit and filter.

8. Acknowledgement

The research described in this paper was carried out at the Jet Propulsion Laboratory, California Institute of Technology, under a contract with the National Aeronautics and Space Administration.

9. References

1. A. A. Stark, R. A. Chamberlin, J. G. Ingalls, J. Cheng, and G. Wright, "Optical and Mechanical Design of the Antarctic Submillimeter Telescope and Remote Observatory," *Rev. Sci. Instrum.*, **68**, 5, 1997.

2. A. K. Tickoo, R. Koul, S. K. Kaul, I. K. Kaul, C. L. Bhat, N. G. Bhatt, M. K. Kothari, H. C. Goyal, N. K. Agrawal, and S. R. Kaul, "Drive-Control System for the TACTIC Gamma-Ray Telescope," *Experimental Astronomy*, **9**, 2, 1999.

3. L. C. Hale and A. H. Slocum, "Design of Anti-Backlash Transmission for Precision Position Control Systems," *Precision Engineering*, **16**, 4, 1994.

4. T. J. Yeh and Y. C. Pan, "Modeling and Identification of Opto-Mechanical Coupling and Backlash Nonlinearity in Optical Disk Drives," *IEEE Transactions on Consumer Electronics*, **46**, 1, 2000.

5. F. R. Boddeke, L. J. VanVliet, and I. T. Young, "Calibration of the Automated z-Axis of a Microscope Using Focus Function," *Journal of Microscopy*, **186**, 3, 1997.

6. S. S. Ku, G. Larsen, and S. Cetinkunt, "Fast Tool Servo Control for Ultra-Precision Machining at Extremely Low Feed Rates," *Mechatronics*, 8, 4, 1998.

7. T. A. Trautt and E. Bayo, "Inverse Dynamics of Flexible Manipulators with Coulomb Friction or Backlash and Non-Zero Initial Conditions," *Dynamics and Control*, **9**, 2, 1999.

8. M. M. Bridges, D. M. Dawson, and J. Hu, "Adaptive Control for a Class of Direct Drive Robot Manipulators," *Int. Journal of Adaptive Control and Signal Processing*, **10**, 4, 1996.

9. R. Dhaouadi, K. Kubo, and M. Tobise, "Analysis and Compensation of Speed Drive Systems with Torsional Loads," *IEEE Transactions on Industry Applications*, **IA-30**, 3, 1994.

10. M. T. Mata-Jimenez, B. Brogliato, and A. Goswami, "On the Control of Mechanical Systems with Dynamics Backlash," *Proceedings of the 36th Conference on Decision and Control*, San Diego, California, 1997.

11. B. Friedland and L. Davis, "Feedback Control of Systems with Parasitic Effects," *Proceedings of the American Control Conference*, Albuquerque, NM, 1997.

12. W. Gawronski and J. A. Mellstrom, "Modeling and Simulations of the DSS 13 Antenna Control System," TDA Progress Report 42-105, 1991 (available at http://tmo.jpl.nasa.gov/tmo/progress_report/42-105/105I.pdf).

13. W. Gawronski and J. A. Mellstrom, "Control and Dynamics of the Deep Space Network Antennas," in C. T. Leondes (ed.), *Control and Dynamic Systems, Volume 63*, San Diego, Academic Press, 1994.

Introducing the Feature Article Authors

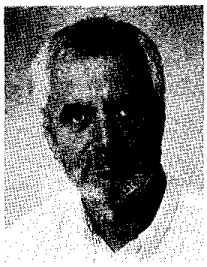

Wodek Gawronski received his MSc and PhD in mechanical engineering from the Technical University of Gdansk, Poland. He was a professor of dynamics and controls at the Technical University of Gdansk and at the University of Hanover, Germany. Later, he was a NRC Senior Fellow at the NASA Langley Research Center, Hampton, Virginia, working on spacecraft structural dynamics and control problems. Currently, he is Engineering Principal in the Communication Ground Systems Section, Jet Propulsion Laboratory, responsible for the control-system analysis and design of the NASA Deep Space Network antennas. He was also a consultant on control-system design to several radio telescope projects, including the NRAO 100-meter Green Bank Telescope, West Virginia, and the 50-meter Large Millimeter Wavelength Telescope in Pueblo, Mexico.

Jason Beech-Brandt graduated with a Bachelor of Science in Mechanical Engineering with a Mathematics Minor from the University of Washington, Seattle, Washington, in 1998. During this time he spent nine months at the Jet Propulsion Laboratory as a co-operative student, working on control and dynamics problems of the Deep Space Network antennas. He is currently working towards a PhD in Mathematics at the University of Edinburgh, Edinburgh, Scotland.

Harlow Ahlstrom graduated from California Polytechnic State University at San Luis Obispo with a bachelors of Science in Electronic Engineering in 1984. He is a senior member of the technical staff at the Jet Propulsion Laboratory, California Institute of Technology, working on antenna servo controls for NASA's Deep Space Network tracking antennas. Through JPL, he has consulted on the new 50 m Large Millimeter Radio Telescope in Mexico. Most recently, he was the Task Leader on the controller upgrades for NASA's Deep Space Network tracking antennas. He has overseen the specification, design, integration, and test of the servo drive systems for all of the new beam-waveguide antennas.

Erin Maneri received her Bachelor of Science degree in Applied Mathematics at Montana State University in 2000. During her cooperative tour at the Jet Propulsion Laboratory, California Institute of Technology, she worked on antenna pointing and tracking tasks. She plans to attend graduate school at MIT, where she will pursue current topics in control systems engineering. She has also engaged in independent research projects funded by Women in Science and Engineering and the National Science Foundation. Erin's other technical interests include mathematical modeling and medical applications of control systems.